

Time- and polarization-resolved optical spectroscopy of colloidal CdSe nanocrystal quantum dots in high magnetic fields

Madalina Furis¹, Jennifer Hollingsworth², Victor I. Klimov², Scott A. Crooker¹

¹*National High Magnetic Field Laboratory, Los Alamos, NM 87545 and*

²*Chemistry Division, Los Alamos National Laboratory, Los Alamos, NM 87545*

(Dated: October 30, 2018)

In an effort to elucidate the *spin* (rather than *charge*) degrees of freedom in colloidal semiconductor nanocrystal quantum dots, we report on a series of static and time-resolved photoluminescence measurements of colloidal CdSe quantum dots in ultra-high magnetic fields up to 45 Tesla. At low temperatures (1.5 K - 40 K), the steady-state photoluminescence (PL) develops a high degree of circular polarization with applied magnetic field, indicating the presence of spin-polarized excitons. Time-resolved PL studies reveal a marked decrease in radiative exciton lifetime with increasing magnetic field and temperature. Except for an initial burst of unpolarized PL immediately following photoexcitation, high-field time-resolved PL measurements reveal a constant degree of circular polarization throughout the entire exciton lifetime, even in the presence of pronounced exciton transfer via Förster energy transfer processes.

PACS numbers:

Introduction

The remarkable optical properties of colloidal semiconductor nanocrystal quantum dots (NQDs) have attracted considerable interest across the chemical-, physical-, and materials science communities in recent years. Most notably, the zero-dimensional nature of the quantum-confined electrons and holes in NQDs leads to discrete, “atomic-like” energy levels, whose ground-state emission can be size-tuned over broad ranges of the visible and infrared spectrum.¹ Furthermore, the nearly perfect and defect-free nanocrystals grown by modern colloidal chemistry methods virtually eliminate non-radiative exciton relaxation, such that quantum yields associated with radiative recombination approach unity.² These optical properties, combined with the flexibility to functionalize the nanocrystal surface, make NQDs suitable for a wide range of biological and optical applications such as light harvesting systems³, biolabeling^{4,5}, light emitting diodes^{6,7,8,9}, or optical amplification and lasing.¹⁰

These attributes and applications are based largely on the charge and energy degrees of freedom of excitons, electrons, and holes in colloidal NQDs. In recent years, however, consideration of the *spin* degrees of freedom of excitons, electrons, and holes in quantum structures has received significant attention in view of potential applications in the new scientific fields of “spintronics” and quantum computation, wherein future generations of functional devices based on spin orientation and spin entanglement have been proposed.^{11,12,13,14} Both epitaxially-grown quantum dots as well as chemically-synthesized colloidal semiconductor quantum dots are candidate material systems for spin-based devices, due in large part to the truly zero-dimensional (and therefore discrete) nature of the quantum-confined exciton states, which leads to long radiative lifetimes¹⁵ at low temperatures and extended spin coherence.¹⁶ Further, the enhancement of the electron-hole exchange interaction in NQDs lifts the exciton spin degeneracy, such that the ex-

citon ground state in CdSe NQDs, for example, is characterized by a total spin $J = 2$, which is optically forbidden, or “dark”, in the dipole approximation.^{17,18,19,20} Much can be learned about these dark excitons through time- and polarization-resolved optical studies at high magnetic fields, where dark excitons become mixed with optically allowed (“bright”, $J = 1$) states. Since significant mixing occurs only when the exciton Zeeman energy ($E_Z = g_{ex}\mu_B B$) is comparable to the bright-dark energy splitting ($\Delta_{bd} > 10$ meV in small NQDs), magnetic fields on the order of 50 T are typically required to obtain sufficiently strong mixing between different spin excitonic states. Here, g_{ex} is the exciton Lande g-factor, μ_B is the Bohr magneton, and B is the magnetic field in Tesla.

In this paper, we present the results of a detailed polarization and time-resolved magneto-photoluminescence study of colloidal CdSe NQDs in high magnetic fields to 45 T. The photoluminescence (PL) from these nanocrystals is characterized by a high degree of circular polarization in large magnetic fields, indicating the presence of spin-polarized excitons. The measured polarization is shown to be consistent with excitons that are thermally distributed amongst Zeeman-split exciton spin levels. Aside from an initial burst of unpolarized PL, the measured degree of circular polarization remains constant throughout the entire exciton lifetime, even in the presence of strong inter-dot exciton transfer via the Förster energy transfer mechanism. Exciton radiative lifetimes are markedly reduced with applied magnetic field, illustrating the field-induced mixing of the long-lived dark (spin-2) exciton ground state with higher-energy, optically-allowed (spin-1) exciton states.

Experimental Section

Nanocrystal Synthesis. The data presented in this paper are derived from three NQD samples of different size. Colloidal CdSe NQDs of 26 Å and 40 Å diameter were grown by organo-metallic synthesis, following the methods of Murray and co-workers.²¹ The cation and

anion precursors, Me_2Cd and $(\text{TMS})_2\text{Se}$, were combined and injected in a heated ($200\text{ }^\circ\text{C}$) trioctylphosphine oxide (TOPO) solution. The reaction mixture is heated to temperatures varying between $230\text{ }^\circ\text{C}$ and $260\text{ }^\circ\text{C}$ for a few hours. These two NQD samples were overcoated with ZnS through a similar reaction for improved surface passivation and increased PL quantum yield. In addition to acting as a solvent, the TOPO also served as a surfactant, providing solubility. Several precipitations of the NQDs with methanol were carried out in order to remove all excess unbound ligand, and the NQDs were then re-dispersed in hexane. A third sample of as-grown 57 \AA diameter NQDs (no ZnS overcoat) was also prepared through similar methods. For the experiments in high magnetic fields, the samples were prepared by drop-casting NQDs from hexane/octane solutions onto glass slides, forming high quality, optically clear NQD films.

Static Photoluminescence in Pulsed Magnetic Fields. PL spectra in high magnetic fields were acquired at the National High Magnetic Field Laboratory (Los Alamos), using a 50 T pulsed magnet. This magnet provides pulses of roughly 300 millisecond duration, and is powered by a 1.6 megajoule capacitor bank (10 kVolt, 32 milliFarads). For studies at temperatures between 1.5 K and 4 K, the NQD samples were mounted on a fiber-optic probe and loaded directly in the (pumped) liquid volume of a helium bath cryostat. For temperatures above 4 K, the sample probe was loaded into an additional vacuum jacket and backfilled with helium exchange gas. A single 600 micron diameter optical fiber couples 442 nm excitation light from a helium-cadmium laser (Kimmon Electric Co.) to the sample. The same fiber also serves to collect the emitted PL and direct it to a spectrometer. Thin-film circular polarizers sandwiched between the fiber and the sample permit polarization analysis of the PL. The collected PL is dispersed in a 300 mm spectrometer (Acton 308) and detected with a high resolution, liquid-nitrogen cooled CCD camera capable of continuous acquisition of spectra at rates up to 1 kHz (Princeton Instruments, 1340x100 pixel array). In this way, the complete magnetic field dependence of the PL is acquired during each magnet pulse, with roughly 1 hour between magnet pulses.²²

Time-Resolved Photoluminescence in dc Magnetic Fields. Time-resolved PL measurements were performed in the variable-temperature insert of an 18 T superconducting magnet (Oxford Instruments), using techniques and hardware for time-correlated single-photon counting (Picoquant SPC-430). Here, the NQDs were excited at 410 nm by a frequency-doubled ultrafast Ti:sapphire laser (Coherent Mira 900) equipped with an external pulse-picker to reduce the repetition rate.³ The PL was spectrally filtered in a 275 mm spectrometer (Acton 275) to a narrow ($< 1\text{ nm}$) bandwidth, and was detected with a multichannel-plate photomultiplier tube (Hamamatsu R3809U-51). Modal dispersion in the long (25 meter) multimode optical fiber limited the system time resolution to $\sim 500\text{ ps}$.

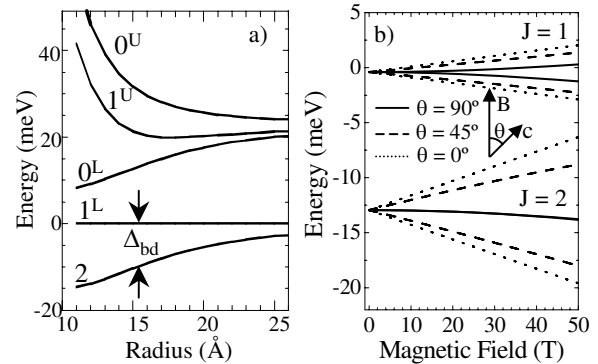


FIG. 1: (a) “Fine structure” of the ground state exciton in CdSe nanocrystal quantum dots (NQDs) as a function of dot radius. The energy levels are labelled by the net spin projection J along the symmetry-breaking crystalline c -axis of the wurtzite NQD. (from ref. 17) (b) Calculated Zeeman splitting of the two lowest exciton levels ($J = \pm 2$, and $J = (\pm 1)^L$) in CdSe NQDs as a function of magnetic field B , for three orientations of the nanocrystal c -axis with respect to the applied field ($\theta = 0, 45$, and 90 degrees). (following ref. 23)

Results and Discussion

Exciton “Fine Structure” in NQDs. Experimental and theoretical studies have established that the enhanced electron-hole exchange interaction in wurtzite CdSe NQDs lifts the spin degeneracy of the band-edge exciton.^{17,18,19,20} The result, shown in Figure 1a, is a five-level exciton “fine structure”, in which the five states are characterized by their total spin projection J along the symmetry-breaking crystalline c -axis of the wurtzite NQD.^{17,23} In prolate or spherical NQDs, the lowest (ground state) exciton has spin projection $J = 2$, which therefore cannot couple directly to light (photons having spin equal to 1). This $J = 2$ dark exciton resides 2-18 meV (depending on NQD size) below the lowest optically allowed ($J = 1^L$), bright exciton state.¹⁹ The evolution of this bright-dark energy gap, Δ_{bd} , as a function of NQD size can be seen in Figure 1a. Within this framework and in the absence of external magnetic fields, previous studies¹⁵ have shown that the radiative recombination of $J = 2$ dark excitons occurs either via thermal activation to the lowest optically-allowed state ($J = 1^L$), or at the lowest temperatures, through higher-order processes such as LO phonon assisted transitions. (In this case, the LO phonon carries away the extra unit of angular momentum).

Application of an external magnetic field allows for direct radiative recombination of dark excitons, due to field-induced mixing between the dark and bright exciton states.¹⁹ As described by Efros²³, the degree of bright-dark mixing depends critically on the orientation of the applied magnetic field with respect to the crystalline c -axis of the NQD. In zero magnetic field, exciton spins are naturally aligned (and quantized along) the c -axis of the wurtzite NQD. Magnetic fields exactly parallel to the c -

axis cause no bright-dark mixing, and the \mathbf{c} -axis remains a good spin quantization axis. Parallel magnetic fields result in the usual Zeeman spin splitting of $J = (\pm 1)^L$ and $J = \pm 2$ excitons. In contrast, magnetic fields orthogonal to the NQD \mathbf{c} -axis strongly mix the lowest $J = \pm 2$ dark states with the optically active $J = (\pm 1)^L$ excitons (*i.e.*, the \mathbf{c} -axis is no longer a valid spin quantization axis). This mixing allows PL emission directly from the lowest exciton states, leading to a faster exciton decay even at low temperature. No Zeeman splitting of the $J = \pm 2$ exciton states is induced, to first order, for fields exactly orthogonal to the \mathbf{c} -axis. In general (see Figure 1b), for an NQD having its \mathbf{c} -axis at an angle θ with respect to the applied magnetic field, the parallel component of the magnetic field, $B \cos \theta$, generates a Zeeman splitting of the states, while the perpendicular component of the magnetic field, $B \sin \theta$, induces mixing between the dark and bright states. In an actual ensemble, the NQDs have random orientation, so that quantitative interpretation of magneto-optical data requires proper averaging over all possible NQD orientations.

Circularly-Polarized Photoluminescence in Ultrahigh Magnetic Fields. Figure 2 shows characteristic polarization-resolved PL spectra from NQDs at low temperatures. These data show the 1.6 K PL spectra from the sample of 26 Å NQDs, in both right (σ^+) and left (σ^-) circular polarizations, at 0, 15, 30, and 45 T collected in the Faraday geometry (\mathbf{B} parallel to the incident light direction). At this temperature, the zero-field PL from these small NQDs is peaked at 2.41 eV and has a full width at half-maximum (FWHM) of ~ 100 meV, due to the 5% dispersion of NQD size in the sample. With increasing magnetic field, the data show a significant degree of circular polarization. The intensity of the σ^- emission increases steadily with applied magnetic field, while emission from the opposite circular polarization (σ^+) decreases with field and remains roughly constant above 15 T. The marked circular polarization that develops with applied magnetic field indicates the presence of predominantly spin-polarized excitons in the NQDs. Only small changes in the PL linewidth are observed. Further, although magnetic fields dramatically reduce the observed PL lifetimes (to be shown later), the time- and polarization-integrated PL emission varies only by $\sim 10\%$ as a function of magnetic field - again indicating the nearly complete absence of competing nonradiative recombination channels in these NQDs.

The complete field- and polarization-dependent intensities for the same 26 Å NQDs are shown in Figures 3a-d, at 1.6, 4.0, 10, and 20 K. At the lowest temperatures (Figure 3a), the intensity of the σ^- emission grows steadily, increasing by a factor of 1.75 at the maximum applied magnetic field of 45 T, while the intensity of the σ^+ emission decreases to half its initial value by 10 T and remains roughly constant thereafter. At higher temperatures to 20 K, these intensity shifts remain qualitatively the same, but are reduced somewhat in magnitude. The corresponding peak energies of the PL are shown in Fig-

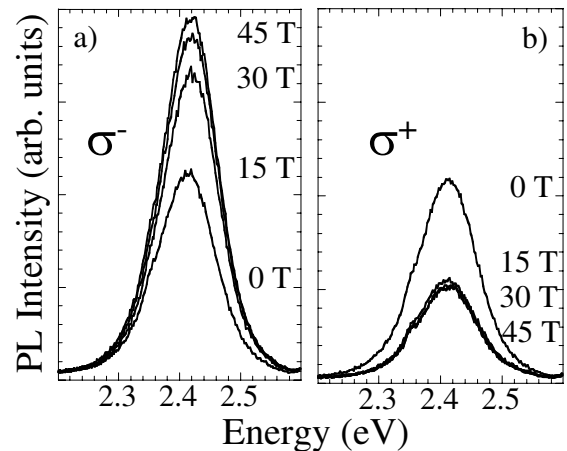


FIG. 2: Photoluminescence (PL) spectra acquired at 1.6 K from the 26 Å diameter CdSe/ZnS NQDs at 0, 15, 30, and 45 T in both (a) σ^- and (b) σ^+ circular polarizations.

ures 3e-h. At higher temperatures (4 K - 20 K), the zero-field PL is peaked at 2.419 eV. With applied field, both σ^+ and σ^- emission peaks exhibit a monotonic redshift toward lower energies, with the σ^+ emission showing a larger energy shift, leading to a small but apparent splitting between the two opposite circular polarizations. At the lowest temperature (*i.e.*, the 1.6 K data of Figure 3e), the zero-field PL appears at slightly lower energy (2.411 eV), due to an increased probability of phonon-assisted emission from these dark excitons.¹⁹ The subsequent non-monotonic energy shifts observed between 0 and 20 T result from the field-induced mixing of dark excitons with higher-energy bright-exciton states, increasing the likelihood of direct recombination without involvement of phonons.

It is notable that the intensity of the σ^+ PL emission does not approach zero at high magnetic fields, but rather saturates at a finite value (see Figures 3a-d). This behavior is a direct result of the random orientation of NQD \mathbf{c} -axis (with respect to the applied magnetic field) in the sample. Following the ideas of Efros and Johnston-Halperin^{23,24}, this data can be qualitatively modelled by considering circularly-polarized emission from randomly-oriented NQDs containing a thermal population of $J = \pm 2$ dark excitons. In the present Faraday geometry, spin-polarized excitons in an NQD with the \mathbf{c} -axis oriented at an angle θ to the applied field will emit σ^+ light with intensity proportional to $(1 + \cos \theta)^2$, and σ^- light with intensity proportional to $(1 - \cos \theta)^2$. For oppositely-oriented excitons, these intensities are reversed: $(1 - \cos \theta)^2$ for σ^+ light, and $(1 + \cos \theta)^2$ for σ^- light. Note, therefore, that NQDs with \mathbf{c} -axis parallel to the applied field ($\theta = 0$) emit 100% circularly polarized light along the direction of observation, but that NQDs with \mathbf{c} -axis orthogonal to the applied field ($\theta = 90$ degrees) emit unpolarized light along the direction of observation. Boltzmann (thermal) statistics

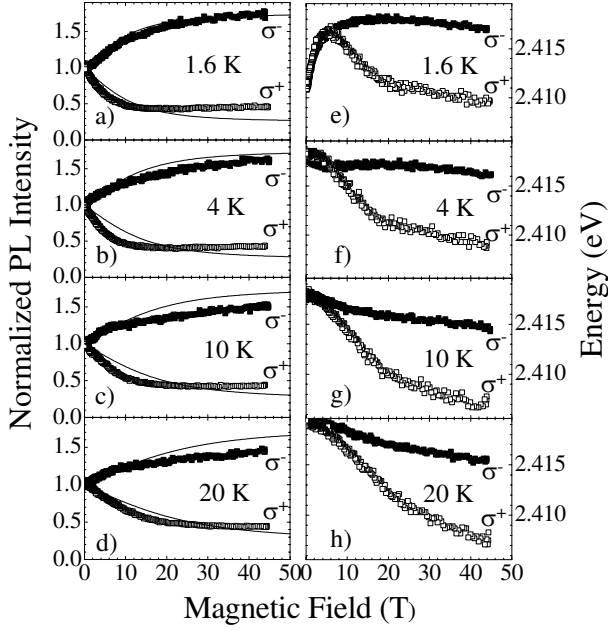


FIG. 3: (a-d) Integrated intensities of the σ^- and σ^+ PL emission as a function of applied magnetic field, at the temperatures indicated, in the 26 Å CdSe/ZnS NQDs. The continuous lines represent the expected evolution of the σ^- and σ^+ components of the emission from randomly-oriented NQDs containing a thermal population of $J = -2$ and $J = +2$ dark excitons as described by Equations (1) and (2). (e-h) Corresponding energy of the PL emission peak, showing splitting between σ^- and σ^+ components, and markedly non-monotonic behavior at the lowest temperatures.

determines the relative population of $J = \pm 2$ excitons, given the orientation-dependent $J = \pm 2$ Zeeman spin splitting $E_Z = g_{ex}\mu_B B \cos\theta$, where g_{ex} is the dark exciton g-factor. Letting $x = \cos\theta$ and $\beta = (k_B T)^{-1}$, the angle-dependent intensities of emitted σ^- and σ^+ light are:

$$I_{\sigma^-}(x) = 1 + x^2 + 2x \tanh(E_Z \beta / 2) \quad (1)$$

$$I_{\sigma^+}(x) = 1 + x^2 - 2x \tanh(E_Z \beta / 2) \quad (2)$$

Integrating I_{σ^-} and I_{σ^+} over all NQD orientations ($0 < x < 1$) gives the total PL intensities, which are shown for comparison by the lines in Figure 3a. Note that the predicted σ^+ intensity saturates at a finite value even in the limit of high magnetic fields. Imperfect agreement between the measured data and the straightforward model outlined above likely originates in the exact role played by phonon-replica emission (*i.e.* the contribution of the phonon-replicas to the PL spectrum), and the strong dependence of the dark exciton recombination rate on the magnetic field as a result of the mixing with $J = 1$ bright states. While the overall trends and significant features in the field-dependent intensity may be understood within this model, additional theoretical efforts are

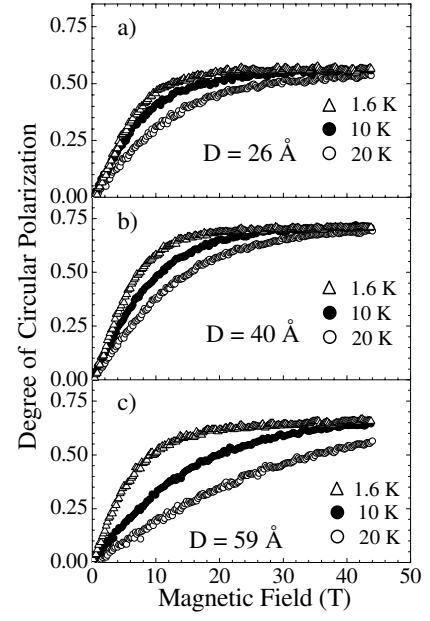


FIG. 4: Degree of circular polarization versus applied magnetic field at 1.6 K, 10 K, and 20 K in the (a) 26 Å CdSe/ZnS NQDs, (b) 40 Å CdSe/ZnS NQDs, and (c) the 57 Å CdSe/TOPO NQDs.

required to elucidate the differences.

From the data of Figures 3a-d, the degree of circular polarization of the PL emission, $P = (I_{\sigma^-} - I_{\sigma^+}) / (I_{\sigma^-} + I_{\sigma^+})$, can be computed as a function of magnetic field. This polarization is shown in Figure 4 at 1.6 K, 4.0 K, 10 K, and 20 K for all three sizes of NQDs. The finite intensity of σ^+ emission (even at the highest magnetic fields) leads to saturation of the degree of circular polarization at a value less than 100%. The temperature dependence of the polarization also follows the behavior of a Boltzmann population of dark excitons, similar to previous studies.²⁴

Time-Resolved Photoluminescence Studies in High Magnetic Fields. We turn now to explicit measurements of the magnetic field dependence of recombination dynamics in CdSe NQDs. As previously established^{15,18,19}, the measured radiative lifetime (τ_R) of excitons in NQDs becomes very long - of order of 1 μ s - at low temperatures below 4 K, as compared with $\tau_R \sim 20$ ns at room temperature. This dramatic increase in τ_R is due to the fact that, below 4 K, excitons are largely frozen out in the $J = 2$ dark exciton ground state, from which direct radiative recombination is forbidden to leading order. As discussed above, these dark excitons eventually undergo radiative recombination through phonon-assisted (or other weakly allowed) processes, in which the phonon takes away the additional quantum of angular momentum. These slow “higher-order” recombination processes ultimately limit τ_R to 1 μ s at low temperatures.

While $J = 2$ exciton states also exist in bulk semi-

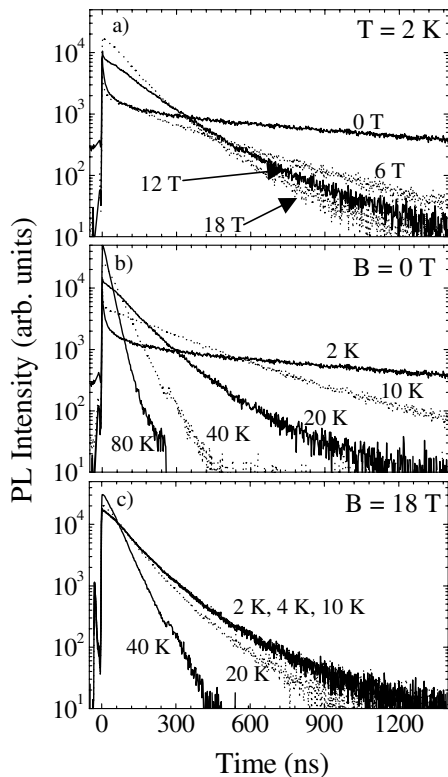


FIG. 5: Time-resolved PL decays (log scale) from the 26 Å CdSe/ZnS NQDs, for (a) different applied fields at 2 K, (b) different temperatures at 0 T, and (c) for different temperatures at 18 T (here, note that the lifetime does not change until 20 K).

conductors and 2-dimensional quantum well systems, the energy splitting between dark and bright states is typically very small ($\Delta_{bd} \sim 0.1$ meV)²⁵, so that even at very low temperatures of order 1 K, the thermal energy, $k_B T \sim 0.09$ meV, is comparable to Δ_{bd} . Thus, thermal excitation of dark excitons to short-lived bright exciton states dominates, and the exciton lifetime in bulk or 2D semiconductors remains fast. In contrast, the bright-dark splitting in NQDs is quite large ($\Delta_{bd} \sim 2 - 18$ meV), so that appreciable thermal excitation of dark to bright excitons, and a correspondingly fast radiative lifetime, is observed¹⁵ only when the thermal energy $k_B T$ approaches Δ_{bd} (practically, at temperatures of a few Kelvin).

In analogy with the case of increased temperature, applied magnetic fields also accelerate the radiative recombination of dark excitons due to field-induced mixing of dark and bright exciton states for those NQDs whose \mathbf{c} -axes are not exactly aligned along \mathbf{B} .^{19,23,24} This effect becomes appreciable when the magnetic (Zeeman) energy $g_{ex}\mu_B B$ approaches Δ_{bd} (practically, at fields of a few Tesla). Thus, the effect of applied magnetic field on the PL dynamics of NQDs is expected to be qualitatively similar to the effect of increased temperature. This comparison is shown explicitly in Figure 5. Figure 5a shows

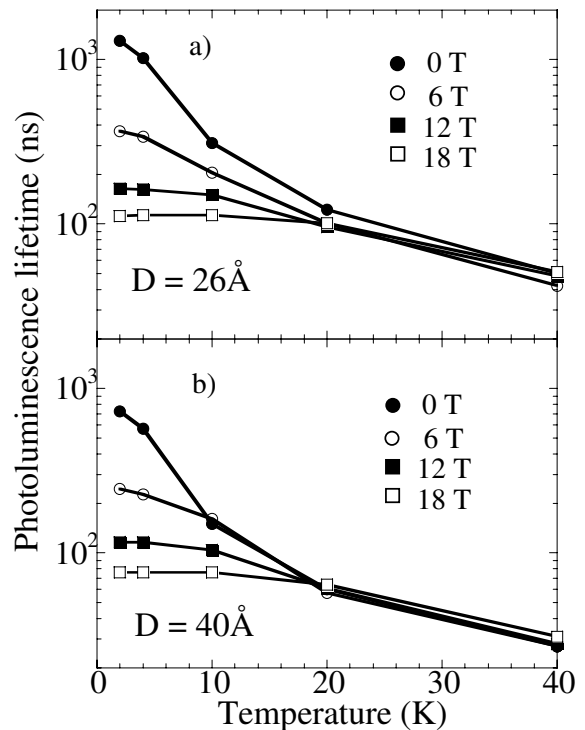


FIG. 6: (a) Measured PL lifetimes versus temperature, at different magnetic fields in (a) 26 Å CdSe/ZnS NQDs and (b) 40 Å CdSe/ZnS NQDs.

PL decays from the 26 Å dots at low temperature (2 K), at 0, 6, 12, and 18 Tesla. With increasing magnetic field, the PL lifetime becomes shorter, decreasing from $\sim 1 \mu\text{s}$ at 0 T to ~ 100 ns at 18 T, consistent with field-induced mixing of dark and bright exciton states. We note that the measured PL decays in applied magnetic field are expected to be non-exponential, as they contain contributions from randomly-oriented NQDs (each particular NQD orientation gives a particular amount of bright-dark mixing, and thus a particular radiative lifetime). Nonetheless, the data of Figure 5a show that the PL dynamics at long delays (hundreds of nanoseconds) are largely exponential, and for the purposes of empirical comparison, can be characterized by a single radiative lifetime. Figure 5b shows the similar effect of increased temperature on PL dynamics. Here, at zero applied magnetic field, increasing temperature accelerates the PL radiative decay due to thermal activation of dark to bright exciton states, as discussed above and observed previously.¹⁵ These data show that the lifetime is reduced from $\sim 1 \mu\text{s}$ at 2 K to ~ 100 ns at 20 K, similar to the effect of an 18 T applied magnetic field. When both magnetic fields and elevated temperatures are present, the PL radiative lifetime is therefore limited primarily by the larger of the two energy scales ($k_B T$ or $g_{ex}\mu_B B$), as shown in Figure 5c. These data show that at 18 Tesla, the PL lifetime remains unchanged by increases in temperature, until it rises above a temperature of ~ 20 K.

The interplay between the effects of temperature and applied field on PL lifetime are summarized in Figure 6, where the measured PL lifetimes are shown for the 26 Å and 40 Å NQDs as a function of both temperature and magnetic field. As can be seen, application of an 18 T magnetic field at the lowest temperatures reduces the radiative lifetime by an order of magnitude, whereas increasing the temperature while in the presence of high magnetic fields has little effect on the PL lifetime. We note again that the time- and polarization-integrated PL intensity remains virtually unchanged by increasing magnetic field or increasing temperature (despite the large changes in PL lifetime), indicating the near-absence of competing non-radiative recombination processes.

Dynamic Circular Polarization. Immediately following excitation of NQDs by the pulsed laser, the photo-injected excitons undergo rapid (sub-picosecond to picosecond timescale) energy relaxation down to the band-edge²⁶, and distribute themselves among the Zeeman-split spin states of the lowest exciton level. The static, circularly-polarized PL measurements shown in the previous section are consistent with a Boltzmann thermal distribution of excitons. Time-resolved polarized PL measurements, shown in Figure 7, demonstrate that the degree of PL circular polarization (and therefore exciton spin polarization) is constant throughout the long exciton lifetime. Figure 7 shows decays of the σ^+ and σ^- PL components from the 26 Å NQDs at $B = 18$ T, at both 2 K and 20 K. PL decays at 0 T are also shown for comparison. This observation suggests that the process of exciton thermalization between states with different spins occurs on a timescale that is considerably shorter than the exciton lifetime.

At very early time delays (< 1 ns), immediately following photoexcitation, the data do reveal a fast, unpolarized component of the PL emission. Figure 8a shows polarization-resolved PL decays at 2 K and at 12 T, where the σ^+ and σ^- emission intensities are initially nearly equal, before settling down to a constant degree of polarization. This initial burst of unpolarized emission disappears with increasing temperature, as shown in Figure 8b, where the relative amplitude of the initial burst is diminished by 20 K and absent at 40 K. The sub-nanosecond measured timescale of this initial decay is commensurate with the 500 ps system time resolution; thus, it is likely that the dynamics of this unpolarized component are faster. This burst of emission may result from the relaxation of the non-thermal and unpolarized excitons that are photoinjected at ~ 3.0 eV by the pulsed, frequency-doubled Ti:Sapphire laser. As these unpolarized excitons decay in energy towards the lowest dark exciton levels at 2.4 eV, they must relax through the cascade of higher-lying optically-allowed levels, from which the probability for radiative recombination is much larger. Further experiments with improved time resolution are necessary to resolve the timescale of exciton spin thermalization within the manifold of band-edge exciton states.

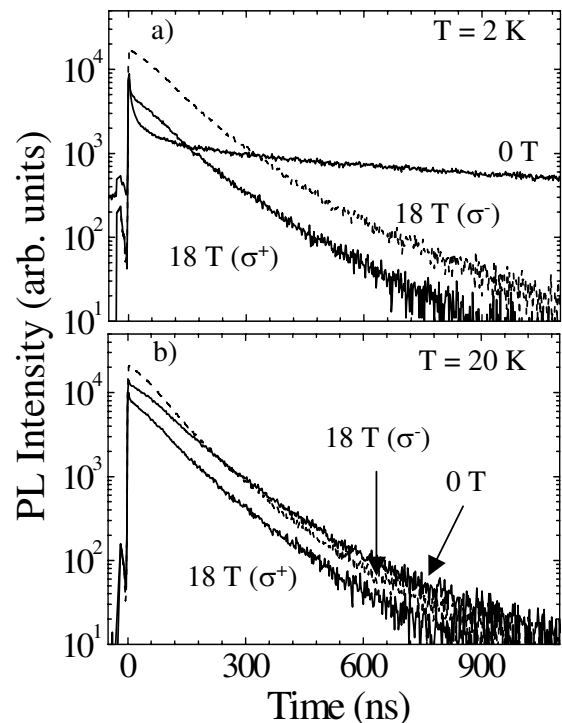


FIG. 7: (Time- and polarization-resolved PL decays in the 26 Å CdSe/ZnS NQDs at 18 T, at (a) 2 K and (b) 20 K, showing constant degree of circular polarization throughout the exciton lifetime

Energy Transfer in Magnetic Fields. Finally, recent experiments have established that inter-dot communication via Förster energy transfer is an effective means of NQD coupling.^{3,27,28} These studies portend favorably for an efficient means of energy and exciton transfer, in applications such as light harvesting, using artificial materials constructed of colloidal NQDs or “non-contact” activation of NQDs using exciton transfer from proximal epitaxial semiconductor layers.⁸ We show in this last section that inter-dot coupling via Förster transfer processes may also preserve exciton spin degrees of freedom; an important characteristic for future “spintronic” devices and applications of quantum computing. Following the measurements of ref. 3, Figure 9a shows time-resolved PL decays at selected wavelengths spanning the inhomogeneously broadened PL emission line, at an intermediate temperature of 40 K. Here, the NQDs in the drop-cast film are close-packed, so that they are sufficiently close together to allow for efficient Förster transfer between dots. When measuring the PL decay on the high energy (short wavelength) side of the PL emission at 2.51 eV, the lifetime is observed to be fast - of order of 20 ns. Emission at this high energy comes from the smallest dots in the ensemble, which have largest band gap. As the detection energy is decreased (moving to longer wavelengths), the measured PL decay becomes longer and longer, eventually reaching a value of ~ 60 ns at 2.31 eV. PL at these longer wavelengths (from the larger

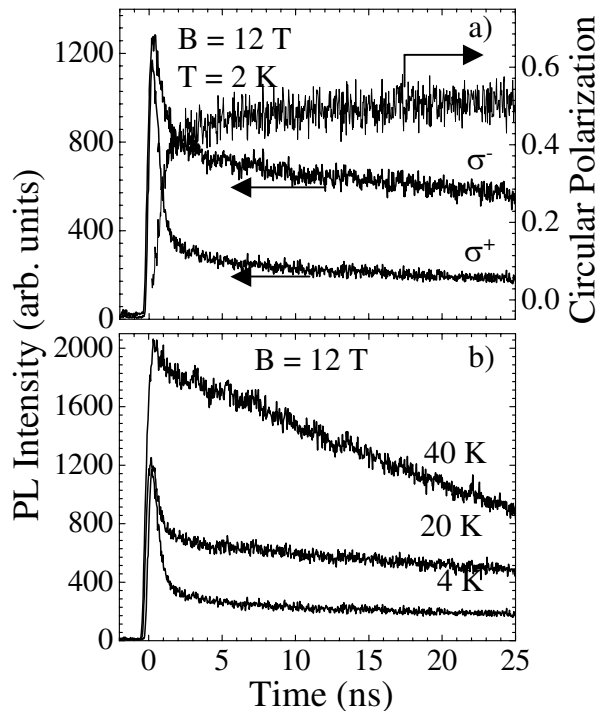


FIG. 8: (a) Expanded view of the polarization-resolved initial PL decay and the circular polarization decay in 26 Å dots at 12 T, showing an unpolarized initial spike at low temperatures (2 K). The width of initial spike is limited by the system response time. (b) Temperature evolution of the initial PL decay, showing that the initial burst of unpolarized PL disappears with increased temperatures.

dots in the ensemble) exhibit decidedly non-exponential decays, even showing a slight increase at short time delays. As discussed previously³, these data result from Förster transfer of excitons from the smaller (donor) NQDs to the larger (acceptor) NQDs in the ensemble. Both the rapid PL decay at high energy, and the slow non-exponential decay at low energy indicates a flow of excitons from small to large NQDs occurring after photoexcitation. In high magnetic fields where the PL emission is circularly polarized, polarization analysis of the PL dynamics in the presence of strong Förster coupling reveals that the observed degree of circular polarization is unaffected by the exciton transfer process. Figure 9b shows that, at 18 T, the degree of circular polarization from the larger “acceptor” NQDs remains essentially unchanged throughout the exciton lifetime, even though the overall shape of the decay indicates that a significant number of excitons are being transferred to these acceptor dots (from donor dots) well after the initial photoexcitation at $t = 0$. These data are consistent with a spin-preserving Förster energy transfer process (in which, *e.g.*, a spin-down exciton in the donor NQD is transferred to a spin-down state in the acceptor NQD). However, because the exciton lifetime is much greater than the spin thermalization time, it is important to note that

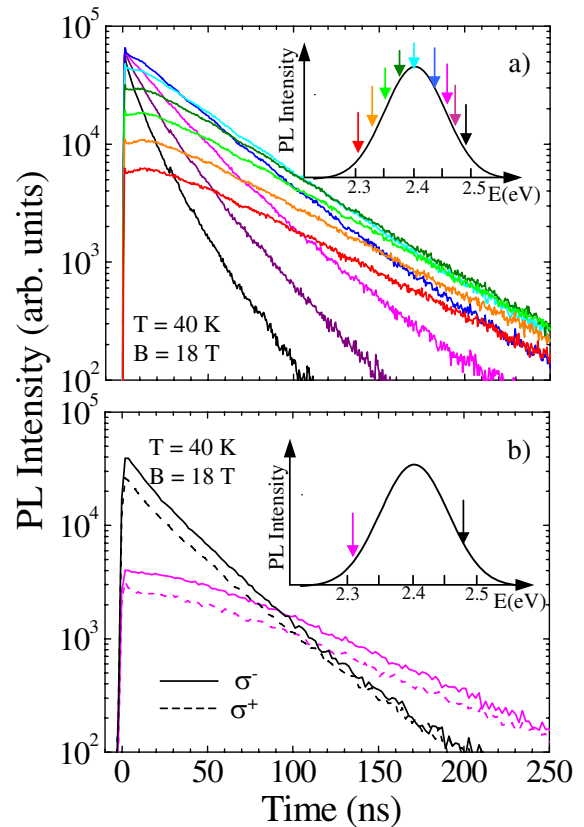


FIG. 9: (a) Time- and spectrally-resolved unpolarized PL decays at selected energies within the PL emission line at 40 K, showing evidence of Förster energy transfer from small NQDs to large NQDs (fast decays at high energies, slow decays at low energies). (b) Polarization-resolved PL decays at 2.47 eV and 2.31 eV, showing that the degree of exciton spin polarization remains constant even in presence of strong Förster energy transfer.

these data do not rule out the possibility that Förster energy transfer is spin-incoherent (and excitons in the acceptor dots become spin polarized by the usual thermalization between Zeeman split states). Nonetheless, recent theoretical work by Govorov²⁹ suggests that spin-coherent transfer of excitons between quantum dots is expected in randomly-oriented quantum dots, particularly if resonance conditions between the donor and acceptor dots are satisfied. As recently proposed, spin-preserving exciton-transfer mechanisms can be exploited for generating quantum entangled states in nanocrystals^{13,30}, as long as the energy transfer is fast enough so that switching between the entangled states occurs on a much faster timescale than the exciton decoherence times.

Conclusions

In conclusion, the spin polarization of excitons in colloidal CdSe NQDs is studied via polarization analysis of the static and time-resolved PL. High magnetic fields lead to a significant degree of circularly polarized PL emission up to 70%, which can be modeled by averaging emission from a thermal distribution between $J = +2$ and

$J = -2$ dark excitons in an ensemble of randomly oriented wurtzite NQDs. Time-resolved studies show that magnetic field induced mixing of dark and bright exciton states leads to markedly reduced exciton lifetimes, quite similar to the effects of thermal excitation from dark to bright exciton states due to increased temperature. Thermalization of photoinjected excitons between

the Zeeman-split $J = \pm 2$ dark exciton states occurs on sub-nanosecond timescales, after which the degree of spin polarization remains constant throughout the exciton lifetime. This constant degree of spin polarization is robust even in the presence of strong inter-dot coupling due to Förster exciton transfer processes.

-
- ¹ Alivisatos, A. P. *Science* **1996**, *271*, 933.
- ² Peng, X.; Schlamp, M. C.; Kadavanich, A. V.; Alivisatos, A. P. *J. Am. Chem. Soc.* **1997**, *119* 7019.
- ³ Crooker, S. A.; Hollingsworth, J. A.; Tretiak, S.; Klimov, V. I. *Phys. Rev. Lett.* **2002**, *89* 186802.
- ⁴ Bruchez, M.; Moronne, M.; Gin, P.; Weiss, S.; Alivisatos, A. P. *Science* **1998**, *281* 2013.
- ⁵ Clapp, A. R.; Medintz, I. L.; Mauro, J. M.; Fisher, B. R.; Bawendi, M. G.; Mattoussi, H. *J. Am. Chem. Soc.* **2004**, *126* 301.
- ⁶ Coe, S.; Woo, W. -K.; Bawendi, M.; Bulcović, V. *Nature* **2002**, *420* 800.
- ⁷ Tessler, N.; Medvedev, V.; Kazes, M.; Kan, S.; Banin, U. *Science* **2002**, *295* 1506.
- ⁸ Achermann, M.; Petruska, M.; Kos, S.; Smith, D. L.; Koleske, D. D.; Klimov, V. I. *Nature* **2004**, *429* 642.
- ⁹ Colvin, V. L.; Schlamp, M. C.; Alivisatos, A. P. *Nature* **1994**, *370* 354.
- ¹⁰ Klimov, V. I.; Mikhailovsky, A. A.; Xu, S.; Malko, A.; Hollingsworth, J. A.; Leatherdale, C. A.; Eisler, H. -J.; Bawendi, M. G. *Science* **2000**, *290* 314.
- ¹¹ DiVincenzo, D. P.; Bacon, D.; Kempe, J.; Burkard, G.; Whaley, K. B. *Nature* **2000**, *408* 339.
- ¹² Imamoglu, A.; Awschalom, D. D.; Burkard, G.; DiVincenzo, D. P.; Loss, D.; Sherwin, M.; Small, A. *Phys. Rev. Lett.* **1999**, *83* 4204.
- ¹³ Lovett, B. W.; Reina, J. H.; Nazir, A.; Briggs, G. A. D. *Phys. Rev. B* **2003**, *68* 205319.
- ¹⁴ Chen, G.; Bonadeo, N. H.; Steel, D. G.; Gammon, D.; Katzer, D. S.; Park, D.; Sham, L. J. *Science* **2000**, *289* 1906.
- ¹⁵ Crooker, S. A.; Barrick, T.; Hollingsworth, J. A.; Klimov, V. I. *Appl. Phys. Lett.* **2003**, *82* 2793.
- ¹⁶ Gupta, J. A.; Awschalom, D. D.; Peng, X.; Alivisatos, A. P. *Phys. Rev. B* **1999**, *59* R10421.
- ¹⁷ Efros, Al. L.; Rosen, M.; Kuno, M.; Nirmal, M.; Norris, D. J.; Bawendi, M. G. *Phys. Rev. B* **1996**, *54* 4843.
- ¹⁸ Nirmal, M.; Murray, C. B.; Bawendi, M. G. *Phys. Rev. B* **1994**, *50* 2293.
- ¹⁹ Nirmal, M.; Norris, D. J.; Kuno, M.; Bawendi, M. G. *Phys. Rev. Lett.* **1995**, *75* 3728.
- ²⁰ Chamarro, M.; Gourdon, C.; Lavallard, P. *J. Lumin.* **1996**, *70* 222.
- ²¹ Murray, C. B.; Norris, D. J.; Bawendi, M. G. *J. Am. Chem. Soc.* **1993**, *115* 8706.
- ²² Crooker, S. A.; Rickel, D. G.; Lyo, S. K.; Samarth, N.; Awschalom, D. D. *Phys. Rev. B* **1999**, *60* R2173.
- ²³ Efros, Al. L., in *Semiconductors and Metal Nanocrystals*, edited by V. I. Klimov (Marcel Dekker Inc., 2004).
- ²⁴ Johnston-Halperin, E.; Awschalom, D. D.; Crooker, S. A.; Efros, Al. L.; Rosen, M.; Peng, X.; Alivisatos, A. P. *Phys. Rev. B* **2001**, *63* 205309.
- ²⁵ Blackwood, E.; Snelling, M. J.; Harley, R. T.; Andrews, S. R.; Foxon, C. T. B. *Phys. Rev. B* **1994**, *50* 14246.
- ²⁶ Klimov, V. I.; McBranch, D. W.; Leatherdale, C. A.; Bawendi, M. G. *Phys. Rev. B* **1999**, *60* 13740.
- ²⁷ Achermann, M.; Petruska, M.; Crooker, S. A.; Klimov, V. I. *J. Phys. Chem. B* **2003**, *107* 13782.
- ²⁸ Kagan, C. R.; Murray, C. B.; Nirmal, M.; Bawendi, M. G. *Phys. Rev. Lett.* **1996**, *76* 1517.
- ²⁹ Govorov, A. O. *Phys. Rev. B* **2003**, *68* 075315.
- ³⁰ Ouyang, M.; Awschalom, D. D. *Science* **2003**, *301* 1074.